Experimental and Theoretical Studies of the Methylidyne CH($X^2\Pi$) Radical Reaction with Ethane (C_2H_6): Overall Rate Constant and Product Channels

Nicolas Galland, Françoise Caralp, Yacine Hannachi, Astrid Bergeat, and Jean-Christophe Loison*

Laboratoire de Physico-Chimie Moléculaire, CNRS UMR 5803, Université Bordeaux I, F-33405 Talence Cedex, France

Received: November 15, 2002; In Final Form: April 25, 2003

The reaction of CH with ethane was studied, at room temperature, in a low-pressure fast-flow reactor. CH($X^2\Pi$, $v = 0$) radicals were obtained from the reactions of $CHBr_3$ with potassium atoms. The overall rate constant is found at 300 K to be $(1.6 \pm 0.6) \times 10^{-10}$ cm^3 molecule^{-1} s^{-1}. The absolute atomic hydrogen production was determined by V.U.V. resonance fluorescence, the reference used being the H production from the CH + CH_4 reaction. The H atoms production from the CH + C_2H_6 reaction was found equal to 22 ± 8%. Ab initio studies of the different stationary points relevant to this reaction and RRKM calculations have been performed for comparison with experimental results.

I. Introduction

The methylidyne radical, CH, is an extremely reactive radical species because of the presence of one singly occupied and one vacant non bonding molecular orbitals localized on the C atom, allowing addition on π bonds and insertion in σ bonds with no barrier. Because of its high reactivity, the CH radical plays an important role in hydrocarbon combustion[1] and in the chemistry of Titan,[2] Neptune,[3] or Triton[4] atmospheres where CH is produced by the photodisssociation of CH_4. The reactions of CH radical are then a potential source of various hydrocarbons, especially ethylene and propene in our case, and could be a way for subsequent production of more complex hydrocarbons.

It is thus interesting to study in detail the kinetics of the CH + C_2H_6 reaction. The possible reaction channels are ($\Delta_r H^0_{298}$ in kJ mol^{-1} [5−10]):

$CH(X^2\Pi) + C_2H_6(X^1A_g) \rightarrow$

i-$C_3H_7(X^2A')$	$\Delta_r H^0_{298} = -425.8 \pm 3.4$
n-$C_3H_7(X^2A')$	-411.6 ± 3.5
$CH_3(X^2A''_2) + C_2H_4(X^1A_{1g})$	-313.5 ± 2.1
$H(^2S) + C_3H_6(X^2A')$ (propene)	-274.2 ± 1.8
$H(^2S) + c-C_3H_6(X^2A')$ (cyclopropane)	-241.1 ± 2.0
$C_3H_5(X^2A') + H_2(X^1\Sigma^+_g)$	-341.7 ± 10.2
$C_2H_3(X^2A') + CH_4(X^1A_g)$	-290.2 ± 4.7
$CH_2(X^3B_1) + C_2H_5(X^2A')$	$+9.9 \pm 7.0$

Despite the great amount of spin allowed accessible channels, only two channels are supposed to play a nimportant rule, formation of hydrogen atoms and propene (H + C_3H_6) and formation of the methyl radical and ethylene (CH_3 + C_2H_4). The first step of this reaction, as in the CH + CH_4 reaction, is the insertion in one of the C−H bond (or/and insertion in the C−C bond) without barrier as the rate constant is growing toward the low temperature down to 23 K.[11] The evolution of the adducts is supposed to lead mainly to H + C_3H_6 and CH_3 + C_2H_4. It is in general agreement that the overall rate constant is around 2×10^{-10} cm^3 molecule^{-1} s^{-1} at 300 K, with a significant temperature dependence over the range 23−652 K.[11,12] However, the branching ratio of this reaction is still unknown. Additionally to the direct interest for Titan atmosphere or combustion chemistry of the CH + C_2H_6 reaction, the subsequent evolution of the high energy distribution propyl adduct formed in this reaction is related to the decomposition of propyl radical in high-temperature processes.[13]

We performed new kinetics experiments using a selective source of CH radicals (from the reaction of $CHBr_3$ with potassium atoms), in a low-pressure fast-flow reactor at room temperature. The overall rate constant obtained by following the decay of CH radicals laser induced fluorescence signal, with the alkane being introduced in excess, the diffusion corrections having been validated in a previous study. Absolute product branching ratios were estimated over the channels yielding H atoms by comparison with the CH + $CH_4 \rightarrow C_2H_4$ + H reaction,[14] with H atoms being probed by resonance fluorescence in the vacuum ultraviolet. New ab initio and RRKM studies were performed in order to assess more precisely the mechanism of this reaction.

II. Theoritical and Experimental Methodology

A. Ab Initio Calculations. The structures of stationary points along the CH ($^2\Pi$) + C_2H_6 ($^1A_{1g}$) reaction have been optimized using the quadratic configuration interaction method including single and double excitations, QCISD,[15] and the hybrid density functional B3LYP[16−18] including nonlocal gradient correction. Both methods were used in conjunction with the correlation consistent polarized valence double-ζ basis set of Dunning and co-workers augmented with diffuse functions, aug-cc-pVDZ.[19] The harmonic vibrational frequencies have been computed at

* To whom correspondence should be addressed. E-mail: jc.loison@lpcm.u-bordeaux1.fr. Fax: (33) 5 57 96 25 21.

10.1021/jp027465r CCC: $25.00
Published on Web 06/21/2003

the B3LYP level of theory in order to characterize the stationary points (minima vs saddle points), to obtain the data needed in the RRKM kinetics study, and to generate the force constant matrix used in the intrinsic reaction coordinate (IRC) calculations. Total energies are refined at the CCSD(T) (coupled cluster with single and double excitations and a perturbational estimate of triple excitations[20,21]) level with the polarized valence triple-ζ cc-pVTZ basis set[22] using B3LYP/aug-cc-pVDZ optimized geometries. The discussed energetics are those obtained at the CCSD(T)/cc-pVTZ//B3LYP/aug-cc-pVDZ level and are corrected with the non scaled B3LYP/aug-cc-pVDZ zero-point vibrational energy (ZPVE). The minimum energy paths were traced at the B3LYP level using the IRC method[23,24] to confirm that the located saddle points connect the presumed minima. For the QCISD and CCSD(T) calculations, the core electrons have been frozen. Unless otherwise noted, the T_1 diagnostic of Lee and co-worker[25] is smaller than the recommended values for closed-shell and open-shell species, respectively 0.02 and 0.03, showing that the multiconfiguration based approach is not necessary to get reliable theoretical data. All calculations have been carried out with the Gaussian 98 program.[26]

B. Experimental Measurement. The experimental setup has been described in detail previously,[27−29] and only a brief summary is given here. The setup consists of a fast-flow reactor, i.e., a 36-mm inner tube with four optical ports for detection. The CH radicals are produced in an "injector" which slides in the reactor. At the end of the injector, the CH radicals are mixed with the ethane flow. Then, the distance (*d*) between the end of the injector and the observation windows is directly proportional to the reaction time. The CH radicals are probed by LIF using a ND:YAG laser (Quantel YG 581C) pumped dye laser (around 100 μJ by pulse) and exciting the CH ($A^2\Delta \leftarrow X^2\Pi$) near 431 nm or by OH ($A^2\Sigma \rightarrow X^2\Pi$) chemiluminescence detection, with electronically excited OH being produced by introducing a very minor amount of O_2 for kinetics experiments (kinetic contribution of the CH + O_2 reaction is always inferior to 5% of the CH + C_2H_6 contribution). The distance (*d*) between the detection windows and the injector nozzle aperture could be varied over the range 0−100 mm with 0.5 mm precision. The pressure was measured by a capacitance manometer (Barocel 0−10 Torr), and the flow rates were adjusted by thermal mass flow controllers. Typically, the pressure was around 1.5 Torr corresponding to a gas speed of 30 m s^{-1}, the reaction time (equal to the distance *d* divided by the gas speed) being comprised between 0 and 3.3 ms.

The CH radicals were produced from the $CHBr_3$ + 3 K → CH + 3 KBr overall reaction which can be separated into three elementary steps ($\Delta_r H^0_{298}$ in kJ.mol^{-1}):[30,31]

$$CHBr_3 + K \rightarrow CHBr_2 + KBr \qquad \Delta_r H^0_{298} = -96 \pm 8 \quad (1)$$

$$CHBr_2 + K \rightarrow CHBr + KBr \qquad \Delta_r H^0_{298} = -75 \pm 8 \quad (2)$$

$$CHBr + K \rightarrow CH + KBr \qquad \Delta_r H^0_{298} = -37 \pm 16 \quad (3)$$

As all of the K + $CHBr_x$ → KH + CBr_x (x ≥ 0) reactions are endoergic, this source can only produce CH radicals. As the sum of the exothermicites of the three abstractions is 208 kJ mol^{-1}, the production of CH($a^4\Sigma^-$) radicals, which is 69.9 kJ mol^{-1} above the ground state, is possible. However that should require high concentration of metastable species with long lifetime (as electronic excited CHBr) in the oven, which is unlikely in our conditions. Moreover, the CH($a^4\Sigma^-$) reactivity is certainly much lower than the CH($X^2\Pi$) reactivity toward C_2H_6.[32]

As a large excess of potassium is introduced in the injector compared to the $CHBr_3$ concentration, the precursors ($CHBr_3$, $CHBr_2$, and CHBr) concentrations in the fast flow reactor are very small and will not interfer in our study, as well as K atoms which are not reactive with ethane molecule. The injector conditions are the following: P = 1.5 Torr, [K] = 1 mTorr, [$CHBr_3$] = 0.05 mTorr, which give in the fast flow reactor: P = 1.5 Torr, [K] < 0.1 mTorr, [$CHBr_3$, $CHBr_2$, and CHBr] ≪ 0.001 mTorr and [CH] ≈ 0.003 mTorr. C_2H_6 was used directly from the cylinder with a purity > 99.995%. $CHBr_3$ (99%) was used without any further purification. Hydrogen atoms were detected by resonance fluorescence using the $2p^1\ ^2P^0 \leftrightarrow 1s^1\ ^2S$ transition at 121.6 nm. Atom excitation was achieved with the microwave discharge lamp previously described.[29] We also used the microwave discharge lamp in an absorption setup to check the absorption of H atoms, ethane and methane in the reactor. Typically the maximum H atoms absorption at the L_α is 3% which correspond to about 4 × 10^{10} molecule cm^{-3}, with our microwave lamp conditions, and the absorptions of methane and ethane are inferior to 0.1%. Thus, the conditions of the presently reported experiments ensure the linear dependence of the atomic fluorescence signal versus the lamp emission intensity and the H atoms concentration, and the negligeable influence of the methane or ethane absorption.

III. Results

A. Potential Energy Surface. The energy diagram along the reaction path is shown in Figure 1, whereas the structures of the different minima are displayed in Figure 2.

1. Relative Stabilities and Structures. The CH + C_2H_6 doublet energy surface exhibits a large number of species with different stoichiometries and spin multiplicities. The most stable species have C_3H_7 stoichiometry: the iso-propyl radical (C_s, $^2A'$) and the *n*-propyl radical (C_1, ^2A). The calculated reaction enthalpy at 298.15 K is −409.8 kJ/mol for the iso-propyl radical and −397.9 kJ/mol for the *n*-propyl radical. The corresponding experimental values are −425.8 and −411.6 kJ/mol, respectively.[5−7] Two species with C_3H_6 stoichiometry can also be produced by the reaction: the propene (C_s, $^1A'$) and the cyclopropane (D_{3h}, $^1A_1'$). Calculations predict the formation of the propene molecule (with an hydrogen atom) to be exothermic by 260.2 kJ/mol, whereas the reaction enthalpy is 34.2 kJ/mol smaller for the cyclopropane. The experimental heats of reaction are respectively −274.2 and −241.1 kJ/mol for the two isomers.[5] The enthalpy difference, 33.1 kJ/mol, agrees very well with the one calculated. The most favorable exit channel corresponds to the simultaneous formation of the ethylene and methyl radical. The calculated reaction enthalpy, 300.9 kJ/mol, is close to the experimental one (−313.5 kJ/mol).[6] In return, the channel leading to ethyl radical and methylene is predicted to be endothermic by 3.0 kJ/mol at 298.15 K, in good agreement with the experimental value of 9.9 kJ/mol.[5,10] CH and C_2H_6 can also react to form the methyl radical with methyl carbene (C_s, $^3A''$), an isomer of ethylene. The reaction enthalpy is predicted to be −8.0 kJ/mol at 298.15 K.

Calculated structures of the reactants and products are shown in Figure 2. The geometrical parameters calculated at the two levels of theory are very close. The largest difference is observed for the addition complex (C_s, $^2A''$). At the QCISD/aug-cc-pVDZ level, this species has a CH bond of 1.503 Å, longer than a typical CH bond and exhibits important Mulliken charges on those carbon and hydrogen atoms (−0.22 and +0.14 e, respectively). For this type of charge-transfer complex, density functional methods are known to overestimate binding energies

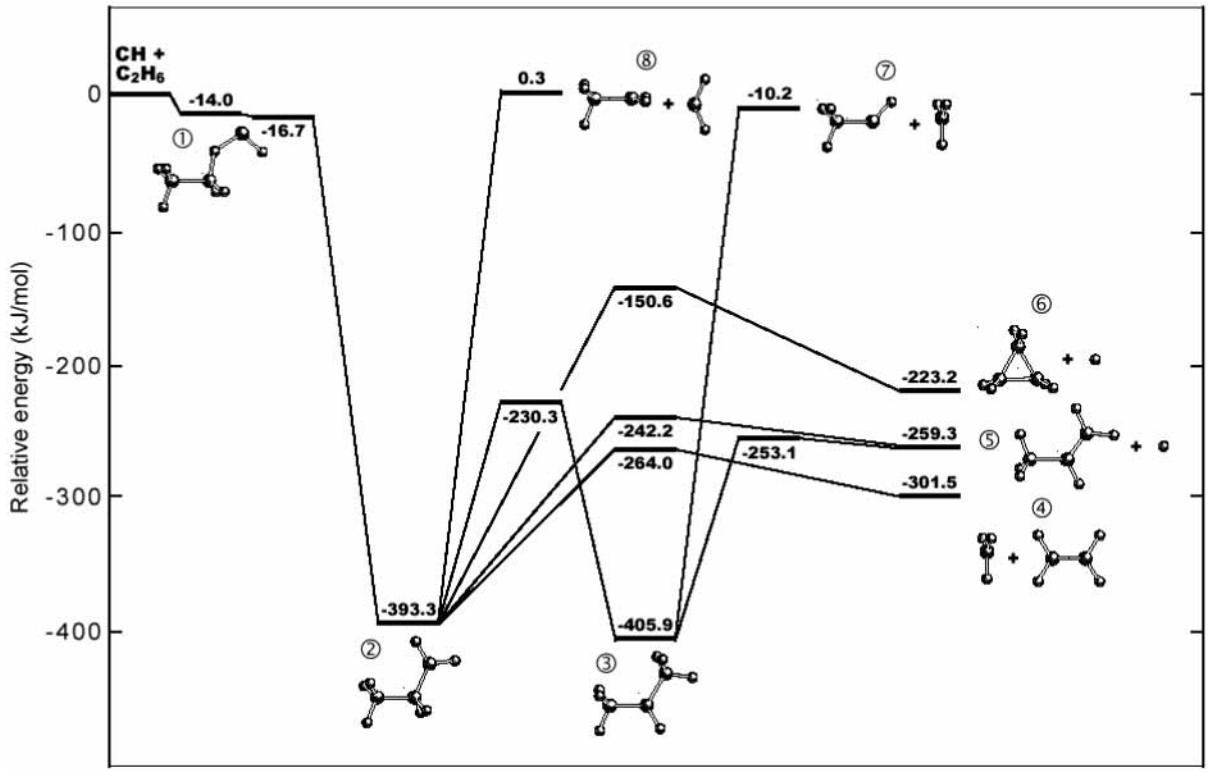

Figure 1. Potential energy diagram for the CH ($^2\Pi$) + C_2H_6 ($^1A_{1g}$) reaction at 0 K. The reported relative energies (kJ/mol) were obtained at the CCSD(T)/cc-pVTZ//B3LYP/aug-cc-pVDZ level with B3LYP/aug-cc-pVDZ ZPVE corrections. The bond orders are not indicated on the schematic structures of the minima.

and underestimate interfragment distances.[33] The CH bond is predicted about 0.17 Å shorter at the B3LYP functional. Experimental geometries are available for almost all of the species,[34−36] and there is a good agreement with the optimized geometries, especially with those obtained at B3LYP/aug-cc-pVDZ level. The discrepancies between experimental and calculated values are within 0.016 (0.024) Å for bond lengths and 0.7° (2.4°) for bond angles at the B3LYP (QCISD) level.

2. Reaction Mechanism. Figure 1 displays a schematic picture of the potential energy surface (PES) correlating with methylidyne CH and ethane C_2H_6 ground states. Two entrance channels have to be considered: insertion of the CH radical into a C−H bond of C_2H_6 leading to the *n*-C_3H_7 (*n*-propyl) radical and insertion of the CH radical into the C−C bond of C_2H_6 leading to the *i*-C_3H_7 (iso-propyl) radical. The first one, leading to the *n*-C_3H_7 radical (species 2) through an addition complex (species 1), is found without any barrier which is in agreement with the large rate constant at low temperature. The relative energy of the addition complex is −14.0 kJ/mol with respect to the reactants. The saddle point (SP1/2) involved in this insertion step is calculated slightly lower than that of species 1 at CCSD(T)/cc-pVTZ//B3LYP/aug-cc-pVDZ, showing that the PES is very flat in the addition complex region. About the second entrance channel, i.e., the insertion of the CH radical in the C−C bond resulting in the formation of *i*-C_3H_7 (species 3), no clear answer has been found, with the search for a reaction pathway being unsuccessfully. However, because of steric hindrance with the CH_3 moiety of ethane and the ability of the two reactants to form species 1, the direct insertion of the CH radical in the CC bond of C_2H_6 is certainly the least favored entrance channel.

Starting from *n*-C_3H_7, several channels are conceivable. First, the *n*-propyl radical can isomerize in the iso-propyl radical (species 3). The barrier for the involved hydrogen shift is of 163.1 kJ/mol. However, in light of the computed PES, the most favorable channels correspond to dissociations leading to C_2H_4 + CH_3 (CC bond breaking; species 4) or CH_3CHCH_2 + H (CH bond breaking of the central carbon; species 5). The respective exit barriers are 129.3 and 151.2 kJ/mol, respectively. Note that the coupled cluster wave function T_1 diagnostics are, for the corresponding saddle points (SP2/4 and SP2/5), slightly larger than the acceptable value of 0.03 recommended by Lee and co-workers.[25] Moreover, activation energies for the reverse reactions C_2H_4 + CH_3 or CH_3CHCH_2 + H → $CH_3CH_2CH_2$ have been found to be 37.8 and 17.9 kJ/mol and could be compared to the Arrhenius parameter from kinetics experiments, 30.8 and 13.6 kJ/mol.[37] The *n*-propyl radical could also dissociate to *c*-C_3H_6 + H through SP2/6 with a barrier of 242.7 kJ/mol. In contrast, the CC bond dissociation of species 2 leading to the methylene and ethyl radical (species 8) is barrier less, but this process is endothermic. Two other highly exothermic exit channels have to be considered for the *n*-C_3H_7 radical evolution, the loss of a H_2 molecule leading to C_3H_5 + H_2 and C−C breaking bond associated with H atom migration leading to CH_4 + C_2H_3. However, attempts to localize saddle points or reaction paths connecting *n*-propyl and those exit channels were unsuccessful. The most favorable channel for the H_2 production is the 1,2-H_2 loss where the hydrogen atoms come from two neighboring carbon atoms. However, the activation energy of this process should be comparable to the barrier of the C_2H_6 → C_2H_4 + H_2 reaction, i.e., 500 kJ mol^{-1} [38], or C_2H_5 → C_2H_3 + H_2 reaction, i.e., 400 kJ mol^{-1}.[14] Thus, even if this channel is energetically accessible, it will not play any rule. About the CH_4 + C_2H_3 production, if there is a mechanism from species 2, it should be concerted and the energy barrier should be certainly much higher than SP2/4 and SP2/5.

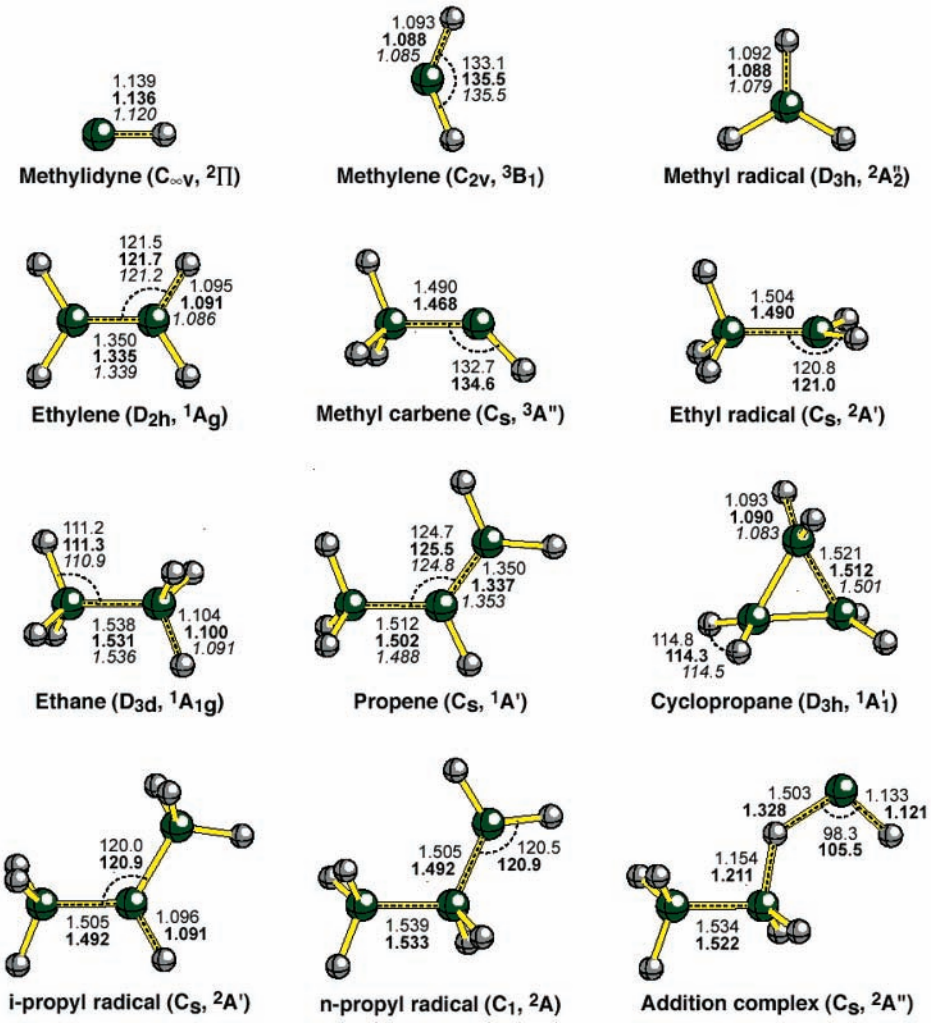

Figure 2. Optimized and experimental structures of minima (distances in angstroms and angles in degrees). The QCISD/aug-cc-pVDZ geometrical parameters are given first, followed by the analogous B3LYP/aug-cc-pVDZ results (in bold type) and experimental data,[34−36] when available (in italic type).

Starting from the *i*-C_3H_7 radical (resulting from the CH radical insertion in the C−C insertion or isomerization of the *n*-C_3H_7 radical), several channels are conceivable. First, the CC bond can dissociate to form CH_3 and CH_3CH (species 7). However, this channel is almost endothermic and will not play any rule in this reaction. Second, the loss of an hydrogen atom could lead to a propene molecule with a computed barrier of 151.2 kJ/mol. For the reverse reaction $CH_3CHCH_2 + H \rightarrow CH_3CHCH_3$, we found a calculated activation energy equal to 8.4 kJ/mol, which could be compared to the Arrhenius parameter from kinetics experiments of 6.5 kJ/mol.[37] This supports the calculated relative stability of SP3/5.

As a consequence, the only observable channels in our experiment are the $H + C_3H_6$ and $CH_3 + C_2H_4$ formation. For the loss of a hydrogen atom leading to cyclopropane, the saddle point (SP2/6) is located much higher than for others exit channels, and it has a much tighter structure. This channel will play a very minor role which is also the case for the isomerization between *i*-C_3H_7 and *n*-C_3H_7. The fact that the isomerization is not favored versus the other exit channels accentuates the importance of the entrance channel (CH or CC insertion). The competition between all of these reaction channels will be discussed in the light of the experimental results and RRKM calculations.

B. Overall Rate Constant. The pseudo-first-order decays of CH radical fluorescence signal were monitored at different concentrations of C_2H_6 introduced in large excess. To get rid of the mixing effects, only the last stages of the decay (after 3 cm from the injector exit) have been taken to determine the pseudo-first-order rate constants. The measured rate constants were then corrected from radial and axial diffusions from Keyser's formula,[39] as done previously with good results.[14]

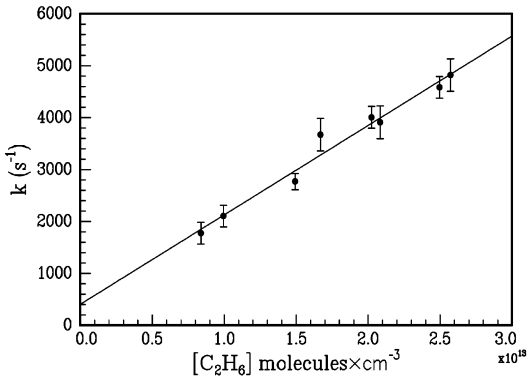

Figure 3. Plot of the pseudo-first-order rate constant of the CH + C_2H_6 reaction versus the C_2H_6 concentration. The gradient of the fitted line yields to the second-order rate constant, $k = (1.6 \pm 0.6) \times 10^{-10}$ cm^3 $molecule^{-1}$ s^{-1}.

TABLE 1: Experimental Enthalpies of Formation at 298 K, in kJ/mol

	expt $\Delta_f H^0$ at 298 K (kJ/mol)
CH	596.4 ± 1.2 [5]
C_2H_6	−84.0 ± 0.2 [5]
n-C_3H_7	100.8 ± 2.1 [5,7]
i-C_3H_7	86.6 ± 2.0 [5,7]
C_2H_4	52.5 ± 0.3 [6]
CH_3	146.4 ± 0.4 [5]
C_3H_6 (propene)	20.2 ± 0.4 [5]
c−C_3H_6 (cyclopropane)	53.3 ± 0.6 [5]
H	218.00 ± 0.01 [6]
CH_4	−74.8 ± 0.3 [5]
C_2H_3	297.0 ± 3.0 [8,9]
C_2H_2	227.7 ± 1.0 [5]
C_2H_5	131.9 ± 2.0 [10]
CH_2	390.4 ± 4.0 [6]
C_3H_5(allyl)	170.7 ± 8.8 [5]

TABLE 2: Experimental and Calculated Reactions Enthalpies at 298 K, in kJ/mol

species	expt 298 K[a]	calcd 298 K [b]
CH($^2\Pi$) + C_2H_6	0	0
n-C_3H_7	−411.6 ± 3.5	−397.9
i-C_3H_7	−425.8 ± 3.4	−409.8
$C_2H_4 + CH_3$	−313.5 ± 2.1	−300.9
$C_3H_6 + H$	−274.2 ± 1.8	−260.2
c−$C_3H_6 + H$	−241.1 ± 2.0	−226.0
$CH_2 + C_2H_5$	+9.9 ± 7.0	+3.0
$CH_3CH + CH_3$		−8.0
$C_3H_5 + H_2$	−341.7 ± 10.2	
$C_2H_3 + CH_4$	−290.2 ± 4.7	

[a] From Table 1. [b] This work.

The results of our experiments are displayed Figure 3, where axial and radial corrected pseudo-first-order rate constant are plotted versus the C_2H_6 concentrations. The main source of errors in our measurements is the important radial and axial diffusions corrections. Moreover, the high wall removal rate constant, because of wall deposit of potassium, associated with these diffusions leads to the limit conditions of the plug-flow approximation and the errors quoted take into account these uncertainties. The second-order rate constant is thus $(1.6 \pm 0.6) \times 10^{-10}$, cm^3 $molecule^{-1}$ s^{-1}, for the CH + C_2H_6 reaction. The present result is in quite good agreement with previous measurements[11,12,40,41] even if it is slightly lower.

C. Product Branching Ratio. Relative hydrogen production of the CH + C_2H_6 was determined on the ratio with the H production from the CH + CH_4 reaction by resonance fluorescence in the vacuum ultraviolet. As the H atoms branching ratio is known for the CH + CH_4 reaction,[14] the determination of the absolute branching ratio for the CH + C_2H_6 reaction can thus be done.

To measure the relative H atoms production, the fluorescence signal is recorded successively for the two reactions CH + CH_4 and CH + C_2H_6. The CH_4 and C_2H_6 concentrations were adjusted in order to have equivalent global first order rate constants, the CH production being constant during a period of more than 1 h. This operation was repeated several times, alternately for different CH_4 and C_2H_6 concentrations, under different pressures and different $CHBr_3$ concentrations. As in our experimental conditions, we cannot neglect secondary reactions, and we performed simulations of H production using reactions detailed in Table 3, including mixing effect and wall reactions, for the three systems: CH alone, CH + CH_4, and CH + C_2H_6, with the parameter to be fitted being the product branching ratio of H atom production of the CH + C_2H_6 reaction. An example of the traces of H atoms concentrations, deduced from the fluorescence signals, versus the distance (i.e. the reaction time) are shown in Figure 4. A simulation is also shown in Figure 4 with a product branching ratio of H production of the CH + C_2H_6 reaction equal to 0.22. The absolute initial concentration of CH radicals has been estimated from the $CHBr_3$ concentration introduced in the oven and also by measuring the H atoms concentration from the CH + CH_4 reaction using atomic resonance absorption spectroscopy and was typically close to 1.0×10^{11} molecules cm^{-3}.

Among the various secondary sources of H atoms, the main one is due to the CH + CH reaction, with contributions from CH + C_2H_4, CH + C_3H_6, and CH + CH_3 reactions. The C_2H contribution is small (quantum chemical studies of $C_2H + CH_4$[42] and $C_2H + C_2H_6$[43] reactions shown than the only accessible channel for these two reactions is direct H atom abstraction). As all secondary H atoms sources involve mainly CH radical reactions with similar H production rate constants for CH_4 and C_2H_6 systems (even if the reactions are different), the estimation of the branching ratio of H production from the CH + C_2H_6

TABLE 3: Reaction Mechanism Used in Simulations of the H Atoms Production for the CH + CH_4 and CH + C_2H_6 Systems

reaction	k_{298K}[a]	ref
CH + CH → C_2H + H	3.0×10^{-10}	Dean et al.[47] Bergeat et al.[28]
CH + C_2H → C_3H + H	3.0×10^{-10}	[b]
CH + CH_4 → C_2H_4 + H	0.9×10^{-10}	Blitz et al.[48] Fleurat-Lessard et al.[14]
CH + C_2H_4 → products	2.8×10^{-10}	Thiesemann et al.[49]
CH + C_2H_4 → C_3H_4 + H	2.0×10^{-10}	Loison[50]
CH + C_2H_6 → C_2H_4 + CH_3	1.3×10^{-10}	This work
CH + C_2H_6 → C_3H_6 + H	0.3×10^{-10}	This work
CH + C_3H_6 → products	2.8×10^{-10}	Loison[50]
CH + C_3H_6 → C_4H_6 + H	1.8×10^{-10}	Loison[50]
CH + CH_3 → C_2H_3 + H	2.0×10^{-10}	[c]
C_2H + CH_4 → C_2H_2 + CH_3	3.0×10^{-12}	Ceursters et al.[42]
C_2H + C_2H_6 → C_2H_2 + C_2H_5	3.5×10^{-11}	Opansky t al[51]
C_2H + C_2H_4 → products	1.2×10^{-10}	Opansky et al.[51]
C_2H + C_2H_4 → C_4H_4 + H	2.0×10^{-11}	Tsang et al.[52]
C_2H + CH_3 → C_3H_3 + H	4.0×10^{-11}	Tsang et al.[52]

[a] In cm^3 $molecule^{-1}$ s^{-1}. [b] Assumed to be equal to CH + CH. [c] Estimated from CH + CH and CH_2 + CH_3 reactions.

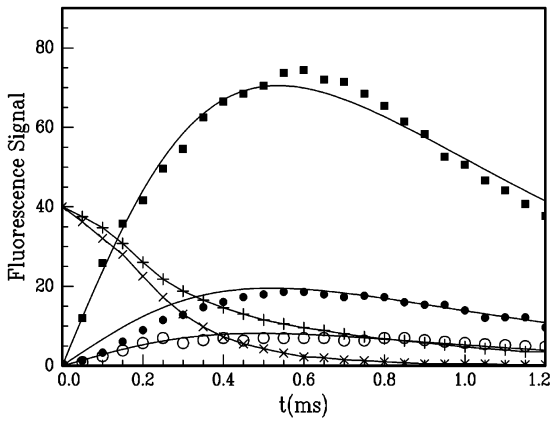

Figure 4. H atoms fluorescence signal, from CH + CH when no co-reactantsis added (circle), from CH + CH_4 (filled box), from CH + C_2H_6 (filled circle) and C_2H* chemiluminescence signal, when no co-reactants are added (plus symbol (+)) and when CH_4 or C_2H_6 is added (cross (×)), in function of the distance *d* in the reactor The fits linking the H production plot result from a global simulation of the different reactions (see text).

TABLE 4: Microcanonical Constants of Different Steps in the Reaction Mechanism at Different Energy, *E*, above the Energy of the Reactants in Their Ground State

steps	2/3	2/4	2/5	2/6	3/2	3/5
k (s^{-1}) ($E = 0$ kJ/mol)	1.31×10^9	1.02×10^{11}	1.16×10^{10}	4.3×10^6	1.06×10^9	7.10×10^{10}
k (s^{-1}) ($E = 4$ kJ/mol)	1.42×10^9	1.09×10^{11}	1.25×10^{10}	5.0×10^6	1.15×10^9	7.63×10^{10}

reaction versus the CH + CH_4 reaction is quite accurate even if the secondary contributions are rather high (typically 10% for CH + CH_4 and 50% for CH + C_2H_6). Based on the study of several experimental runs with various initial CH radical concentrations, we obtained an H product branching ratio of 0.22 ± 0.08 for the CH + C_2H_6 reaction.

D. RRKM Calculations. Considering the results of the ab initio calculations, we limit the system to the following reactions:

$$\begin{aligned}
\mathrm{CH} + \mathrm{C_2H_6} &\rightarrow n\text{-}\mathrm{C_3H_7} \\
&\quad\ i\text{-}\mathrm{C_3H_7} \\
n\text{-}\mathrm{C_3H_7} &\rightarrow \mathrm{CH_3} + \mathrm{C_2H_4} \quad k_{2/4} \\
&\quad\ \mathrm{H} + \mathrm{C_3H_6} \quad k_{2/5} \\
&\quad\ \mathrm{H} + c\text{-}\mathrm{C_3H_6} \quad k_{2/6} \\
n\text{-}\mathrm{C_3H_7} &\rightleftarrows i\text{-}\mathrm{C_3H_7} \quad k_{2/3}, k_{3/2} \\
i\text{-}\mathrm{C_3H_7} &\rightarrow \mathrm{H} + \mathrm{C_3H_6} \quad k_{3/5}
\end{aligned}$$

The microcanonical rate constants of the various steps of the mechanism are obtained from the classical RRKM expression

$$k(E) = \frac{\sigma\, G(E)}{h\, N(E)}$$

In this expression, σ is the symmetry factor, h is the Planck's constant, $G(E)$ is the number of energetically accessible states at the transition state, and $N(E)$ is the density of states of the intermediate species. All species are treated as symmetric tops, and the external K-rotor, associated with the smallest moment of inertia, is treated as an active degree of freedom completely coupled with vibrations.

The initial energy distribution function of the energized adduct radical (i-C_3H_7 or n-C_3H_7) is determined by detailed balance assuming thermal energy distribution on the reactants. Taking into account the narrowness of the thermal energy distribution and the large excess energy in this system, it will be assumed that i-C_3H_7* or n-C_3H_7* are monoenergetically energized with an energy of 4 kJ/mol (350 cm^{-1}) above the reactants in their ground state.

The lifetime τ of the various species for an energy E is then obtained from $1/\tau = \sum_i k_i(E)$, where $k_i(E)$ are the microcanonical constants of all steps in the mechanism in which species i is a reactant. The calculated microcanonical constants of different steps in the mechanism are presented in Table 4. The i-C_3H_7* or n-C_3H_7* RRKM lifetime ($\approx 10^{-11}$ s) meets the ergodicity criterion and is short enough to be able to neglect collisional energy loss (the collision frequency for 1 atm of air at 298 K is $\approx 10^{10}$ s^{-1}). Indeed, chemical activation experiments have enabled the rate constants for randomization to be determined and led to values of the order of 10^{12} s^{-1}.[44]

To calculate the branching ratio, we could consider that each reactive collision between CH and C_2H_6 gives either n-C_3H_7 or i-C_3H_7 with a probability equal respectively to $1 - x$ and x (x being comprise between 0 and 1, depending of the proportion of CH insertion and CC insertion) and solved the following differential equation system:

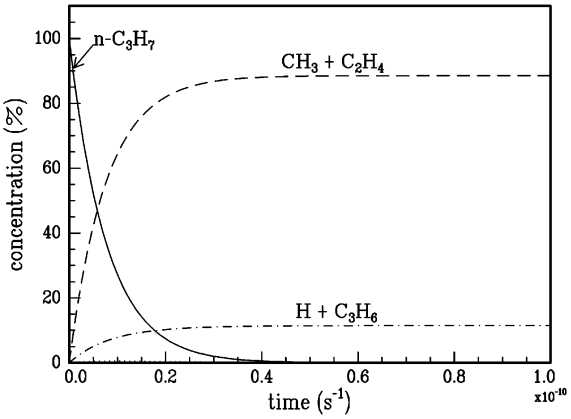

Figure 5. Concentrations of various intermediates and products versus times from RRKM calculation following insertion of CH radical in a C−H bond of ethane.

$$\frac{\mathrm{d}[n\text{-}\mathrm{C_3H_7}]}{\mathrm{d}t} = k_{3/2}[i\text{-}\mathrm{C_3H_7}] - (k_{2/3} + k_{2/4} + k_{2/5} + k_{2/6})[n\text{-}\mathrm{C_3H_7}]$$

$$\frac{\mathrm{d}[i\text{-}\mathrm{C_3H_7}]}{\mathrm{d}t} = k_{2/3}[n\text{-}\mathrm{C_3H_7}] - (k_{3/2} + k_{3/5})[i\text{-}\mathrm{C_3H_7}]$$

$$\frac{\mathrm{d}[\mathrm{H}]}{\mathrm{d}t} = (k_{2/5} + k_{2/6})[n\text{-}\mathrm{C_3H_7}] + k_{3/5}[i\text{-}\mathrm{C_3H_7}]$$

$$\frac{\mathrm{d}[\mathrm{CH_3}]}{\mathrm{d}t} = \frac{\mathrm{d}[\mathrm{C_2H_4}]}{\mathrm{d}t} = k_{2/4}[n\text{-}\mathrm{C_3H_7}]$$

$$\frac{\mathrm{d}[\mathrm{C_3H_6}]}{\mathrm{d}t} = k_{2/5}[n\text{-}\mathrm{C_3H_7}] + k_{3/5}[i\text{-}\mathrm{C_3H_7}]$$

$$\frac{\mathrm{d}[c\text{-}\mathrm{C_3H_6}]}{\mathrm{d}t} = k_{2/6}[n\text{-}\mathrm{C_3H_7}]$$

the initial conditions being $[i\text{-}\mathrm{C_3H_7}]_{t=0} = x$ and $[n\text{-}\mathrm{C_3H_7}]_{t=0} = 1 - x$.

To numerically solve the system, we use the *Bulstoer* (Bulirsch-Stoer) scheme of Mathcad software. We obtained numerical solutions for the amount of the products versus time; the relative amount when they have converged was used for calculations of product branching ratios. Plots of the relative amount versus time for various species are shown in Figure 5 for the evolution n-C3H7 following CH insertion of the CH radical ($x = 0$). The product branching ratios calculated are 88% of CH_3 + C_2H_4 and 12% of H + C_3H_6 following C−H bond insertion of the CH radical. The corresponding values for the C−C bond insertion of the CH radical are 1% of CH_3 + C_2H_4 and 99% of H + C_3H_6. The very small amount of CH_3 + C_2H_4 in the last case is due to the low value of microcanonical rate constant for the isomerization versus the microcanonical rate constant of the other processes. The x factor was adjusted to fit

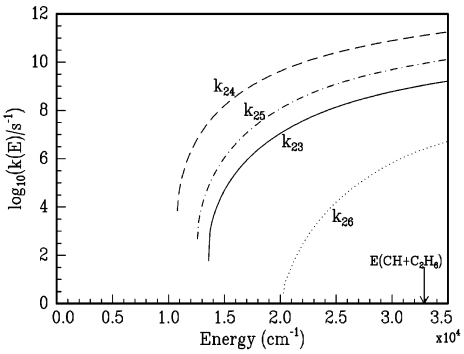

Figure 6. Energy dependencies for microcanonical rate constants of the evolution of the *n*-C_3H_7 radical.

our experimental value of 22% for H atom branching ratio (coming almost exclusively from the H + C_3H_6 exit channel). Thus, we obtained 12% of C−C bond insertion and 88% of C−H bond insertion of the CH radical. If we considered the various sources of uncertainty, for example, by lowering the energy value of the barrier through the SP2/4 and SP2/5 of 4 kJ/mol, we evaluate the precision of RRKM calculations of the product branching ratios to be 6%. The upper limit of the H atom production of *n*-propyl decomposition became 16% and could be compared to the lower limit of the experimental H production which is 14%.

Hence, this H atom production associated with the fact that no reaction path for the C−C insertion of the CH radical could be found in the ab initio calculations, seem indicate that the CH radical insert only in CH bond of C_2H_6 molecule. This result is in agreement with physical consideration such as steric effect, the first step on the insertion of CH radical is the formation of weak H−CH or C−CH bond and the hydrogen atoms are more accessible than C atoms in the C_2H_6 molecule.

E. Comparison with Thermal Decompositions of *n*-Propyl and iso-Propyl Radicals. Products of thermal decomposition of *n*-propyl and iso-propyl radicals have been determined by Yamauchi and co-workers.[13] The H atom yield from the thermal decomposition of *i*-C_3H_7 has been found to be equal to unity, and the H atom yield from the thermal decomposition of *n*-C_3H_7 has been found to be <0.05, within the experimental error limits. In the case of thermal decomposition, the population distribution of internal states for *n*-propyl and iso-propyl radicals are different than in the case of the CH + C_2H_6 reaction were the distribution could be considered as monoenergetically energized. A modified strong collision RRKM calculation of the thermal rate constant at 1000 and 1400 K and 1 atm of N_2 was performed for comparing our products branching ratio of *n*-propyl and iso-propyl decomposition to experimental and theoritical results of Yamauchi.[13] The values of the collision efficiency, β_c, were obtained from the values of the average downward energy transferred by collision, $\langle\Delta E\rangle_{down}$, given by Knyazev and Tsang[45] for dissociation of secondary butyl radical with N_2 as buffer gaz using the expression provided by Troe,[46] $\beta_c = (\langle\Delta E\rangle_{down}/(\langle\Delta E\rangle_{down} + F_E kT))^2$. This returns $\beta_c \cong 0.2$ at 298 K with a slight negative temperature coefficient. We obtain very similar results with the same overestimation of H production for thermal decomposition of *n*-C_3H_7. We also obtain some difference at high temperature where isomerization between iso-propyl and *n*-propyl became non negligible versus C−C bond fission. However, the microcanonical rate constant for this isomerization is always too low to play a substantial role.

In conclusion, we could considered to have a good picture of the CH + C_2H_6 reaction, with mainly insertion of the CH radical in a C−H bond of ethane, and a very minor role for isomerization between iso-propyl and *n*-propyl.

References and Notes

(1) Sanders, W. A.; Lin, M. C. *Chemical Kinetic of Small Organic Radicals*; CRC Press: Boca Raton, FL, 1986; Vol. III.
(2) Wayne, R. P. *Chemistry of Atmospheres*; Clarendon Press: Oxford, U.K., 1991.
(3) Yelle, R. V.; Herbert, F.; Sandel, B. R. *Icarus* **1993**, *104*, 38.
(4) Krasnopolsky, V. A.; Cruikshank, D. P. *J. Geophys. Res. E* **1995**, *100*, 21271.
(5) *Handbook of Chemistry and Physics*; CRC Press: Boca Raton, FL, 2001.
(6) Chase, M. W. J. *NIST-JANAF Themochemical Tables*, 4h ed.; *J. Phys. Chem. Ref. Data* **1998**, *9*.
(7) Tsang, W. *Heats of Formation of Organic Free Radicals by Kinetic Methods in Energetics of Organic Free Radicals*; Blackie Academic and Professional: London, 1996.
(8) Kaiser, E. W.; Wallington, T. J. *J. Phys. Chem.* **1996**, *100*, 4111.
(9) Knyasev, V. D.; Bencsura, A.; Stoliarov, S. I.; Lagle, I. R. *J. Phys. Chem.* **1996**, *100*, 11346.
(10) Berkovitz, J.; Ellison, G. B.; Gutman, D. *J. Phys. Chem.* **1994**, *98*, 2744.
(11) Canosa, A.; Sims, I. R.; Travers, D.; Smith, I. W. M.; Rowe, B. R. *Astron. Astrophys.* **1997**, *323*, 644.
(12) Berman, M. R.; Lin, M. C. *Chem. Phys.* **1983**, *82*, 435.
(13) Yamauchi, N.; Miyoshi, A.; Kosada, K.; Koshi, M.; Matsui, H. *J. Phys. Chem. A* **1999**, *103*, 2723.
(14) Fleurat-Lessard, P.; Rayez, J.-C.; Bergeat, A.; Loison, J.-C. *Chem. Phys.* **2002**, *279*, 87.
(15) Pople, J. A.; Head-Gordon, M.; Raghavachari, K. *J. Chem. Phys.* **1987**, *87*, 5968.
(16) Becke, A. D. *Phys. Rev. A* **1988**, *38*, 3098.
(17) Lee, C.; Yang, W.; Parr, R. G. *Phys. Rev. B* **1988**, *37*, 785.
(18) Becke, A. D. *J. Chem. Phys.* **1993**, *98*, 5648.
(19) Kendall, R. A.; Dunning, T. H., Jr.; Harrison, R. J. *J. Chem. Phys.* **1992**, *96*, 6796.
(20) Purvis, G. D., III.; Bartlett, R. J. *J. Chem. Phys.* **1982**, *76*, 1910.
(21) Raghavachari, K.; Trucks, G. W.; Pople, J. A.; Head-Gordon, M. *Chem. Phys. Lett.* **1989**, *157*, 479.
(22) Dunning, T. H., Jr. *J. Chem. Phys.* **1989**, *90*, 1007.
(23) Fukui, K. *J. Chem. Phys.* **1977**, *66*, 2153.
(24) Gonzalez, C.; Schlegel, H. B. *J. Phys. Chem.* **1990**, *94*, 5523.
(25) Lee, T. J.; Taylor, P. R. *Int. J. Quantum. Chem. Symp.* **1989**, *23*, 199.
(26) Frisch, M. J.; Trucks, G. W.; Schlegel, H. B.; Scuseria, G. E.; Robb, M. A.; Cheeseman, J. R.; Zakrzewski, V. G.; Montgomery, J. A., Jr.; Stratmann, R. E.; Burant, J. C.; Dapprich, S.; Millam, J. M.; Daniels, A. D.; Kudin, K. N.; Strain, M. C.; Farkas, O.; Tomasi, J.; Barone, V.; Cossi, M.; Cammi, R.; Mennucci, B.; Pomelli, C.; Adamo, C.; Clifford, S.; Ochterski, J.; Petersson, G. A.; Ayala, P. Y.; Cui, Q.; Morokuma, K.; Malick, D. K.; Rabuck, A. D.; Raghavachari, K.; Foresman, J. B.; Cioslowski, J.; Ortiz, J. V.; Stefanov, B. B.; Liu, G.; Liashenko, A.; Piskorz, P.; Komaromi, I.; Gomperts, R.; Martin, R. L.; Fox, D. J.; Keith, T.; Al-Laham, M. A.; Peng, C. Y.; Nanayakkara, A.; Gonzalez, C.; Challacombe, M.; Gill, P. M. W.; Johnson, B. G.; Chen, W.; Wong, M. W.; Andres, J. L.; Head-Gordon, M.; Replogle, E. S.; Pople, J. A. *Gaussian 98*, revision A.7; Gaussian, Inc.: Pittsburgh, PA, 1998.
(27) Daugey, N.; Bergeat, A.; Schuck, A.; Caubet, P.; Dorthe, G. *Chem. Phys.* **1997**, *87*, 222.
(28) Bergeat, A.; Calvo, T.; Dorthe, G.; Loison, J.-C. *J. Phys. Chem. A* **1999**, *103*, 6360.
(29) Bergeat, A.; Calvo, T.; Dorthe, G.; Loison, J.-C. *Chem. Phys. Lett.* **1999**, *308*, 7.
(30) Born, M.; Ingemann, S.; Nibbering, N. M. *J. Am. Chem. Soc.* **1994**, *116*, 7210.
(31) Tschuikow-Roux, E.; Paddison, S. *Int. J. Chem. Kinet.* **1987**, *19*, 15.
(32) Hou, Z.; Bayes, K. D. *J. Phys. Chem.* **1993**, *97*, 1896.
(33) Ruiz, E.; Salahub, D. R.; Vela, A. *J. Phys. Chem.* **1996**, *100*, 12265.
(34) Herzberg, G. *Molecular Spectra and Molecular Structures*; D. Van Nostrand Company: New York, 1957; Vol. III.
(35) Kuchitsu, K. *Structure of Free Polyatomic Molecules—Basic Data*; Springer: Berlin, 1998.
(36) Huber, K. P.; Herzberg, G. *Molecular Spectra and Molecular Structures*; D. Van Nostrand Reinhold Co.: New York, 1979; Vol. IV.
(37) Tsang, W. *J. Phys. Chem. Ref. Data* **1991**, *20*, 221.
(38) Gordon, M. S.; Truong, T. N.; Pople, J. A. *Chem. Phys. Lett.* **1986**, *130*, 245.
(39) Keyser, L. F. *J. Phys. Chem.* **1984**, *88*, 4750.
(40) Butler, J. E.; Fleming, J. W.; Goss, L. P.; Lin, M. C. *Am. Chem. Soc. Symp. Ser.* **1980**, *134*, 397.

(41) Butler, J. E.; Fleming, J. W.; Goss, L. P.; Lin, M. C. *Chem. Phys.* **1981**, *56*, 355.
(42) Ceursters, B.; Nguyen, H. M. T.; Peeters, J.; Nguyen, M. T. *Chem. Phys. Lett.* **2000**, *329*, 412.
(43) Ceursters, B.; Nguyen, H. M. T.; Nguyen, M. T.; Peeters, J.; Vereecken, L. *Phys. Chem. Chem. Phys.* **2001**, *3*, 3070.
(44) Holbrook, K. A.; Pilling, M. J.; Roberston, S. H. *Unimolecular Reaction*, 2nd ed.; John Wiley & Sons Ltd.: Chichester, U.K., 1996.
(45) Knyasev, V. D.; Tsang, W. *J. Phys. Chem. A* **2000**, *104*, 10747.
(46) Troe, J. *J. Phys. Chem.* **1977**, *66*, 4715.
(47) Dean, A. J.; Hanson, R. K. *Int. J. Chem. Kinet.* **1992**, *24*, 517.
(48) Blitz, M. A.; Johnson, D. G.; Pesa, M.; Pilling, M. J.; Robertson, S. H.; Seakins, P. W. *J. Chem. Soc.* **1997**, *93*, 1473.
(49) Thiesemann, H.; Clifford, E. P.; Taatjes, C. A.; Klippenstein, S. J. *J. Phys. Chem. A* **2001**, *105*, 5393.
(50) Loison, J.-C. in preparation.
(51) Opansky, B. J.; Leone, S. R. *J. Phys. Chem.* **1996**, *100*, 19904.
(52) Tsang, W.; Hampson, R. F. *J. Phys. Chem. Ref. Data* **1986**, *15*, 1087.